Open Ceramics 13 (2023) 100330

Contents lists available at ScienceDirect

Open Ceramics

journal homepage: www.sciencedirect.com/journal/open-ceramics

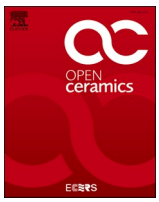

A simple methodology based on numerical analysis for the drying curve design of a castable lined steel ladle

T.M. Cunha [a,*], M.H. Moreira [a], M.F. Santos [a], R.A. Angélico [b], V.C. Pandolfelli [a]

[a] Federal University of São Carlos, Graduate Program in Materials Science and Engineering (PPGCEM), Rod. Washington Luiz, km 235, São Carlos, SP, 13565-905, Brazil

[b] University of São Paulo (USP), Department of Aeronautical Engineering, Av. Trabalhador São-Carlense, 400, São Carlos, SP, 13566-590, Brazil

ARTICLE INFO

Handling Editor: P Colombo

Keywords:
refractory
Castable
Drying
Simulation
Heat-up curve

ABSTRACT

Energy efficiency is closely linked to industry goals of reducing environmental impacts, where selecting the best heating curve has a great effect on the total energy consumption, costs, and CO_2 emission, especially for refractory castable lining equipment. By using numerical modeling, this work analyses the effects of the temperature and heating rate for thermal treatment profiles comprising a single dwell time. Based on the results attained, a single plateau at 350 °C proved not to be useful for lower thickness castable lining (10 cm) as the resistance ratio peak had already reached high values near the beginning of the dwell time. Increasing the castable wall thickness up to 30 cm requires even more complex profiles than the ones presented. In addition to analysing pressure build-up behavior, this work compared the energy efficiency associated with each of the heating curve cases analyzed, providing a methodology for heating schedule selection.

1. Introduction

Refractory ceramics are key materials for the industrial sector as they comprise the lining and thermal insulation of high-temperature equipment, making the production viable of many different products such as glass and steel. They are commonly divided into two groups: shaped and non-shaped. The first has a defined geometry, while the latter is applied directly to the equipment and attains its final shape during the application [1].

For processing non-shaped or a castable ceramic, the material powder must be mixed with a liquid, usually water, and applied to the selected site [2,3]. Due to the moisture content, a controlled heating schedule ensures that the generated vapor within it has enough time to diffuse and leave the material, inhibiting the generation of high pressures that can damage the equipment lining and to reduce operation safety [3].

In a previous published work by the authors on castable drying [4], important parameters such as resistance ratio, which assesses whether a monolithic refractory lining is close to the mechanical failure when subjected to a specific heating curve, the effects of the dynamic permeability and the thermal conductivity under constant heating rate curves, were presented. This was the first step towards optimizing the drying of refractory castables, mainly for steel ladles.

Yet, as it has already been shown, the application of such simple and shorter profiles are limited to the thinner linings (~10 cm monolithic wall), implying that to safely dry more complex geometries or thicker layers, other heating schedules must be evaluated. Usually, the thickness of the working lining of a steel ladle has approximately 20–30 cm, which requires even more controlled and careful pre-heating.

The industry commonly applies plateaus at specific temperatures, to attain a complete and safe drying, where the dwell time length is directly correlated to the thickness of the castable layer [3]. Nevertheless, the practice shows that there is not a specific consensus on how long it should take, whether that temperature is the optimal one, or even if other essential features, such as the kinetics of the drying process, are taken into consideration [5].

This work builds upon the aspects already discussed in the former publication [4], which ensures the safe drying by accounting the resistance ratio for a particular castable composition. It also includes the evaluation of heating up schedules considering the holding times at different temperatures during the drying process, different lining thicknesses, and the effects of different heating rates.

The energy consumption for the different heating profiles is also computed and used as an index to rank the best profiles suited for a given

* Corresponding author.
E-mail address: tulio@dema.ufscar.br (T.M. Cunha).

https://doi.org/10.1016/j.oceram.2023.100330
Received 3 November 2022; Accepted 13 January 2023
Available online 20 January 2023

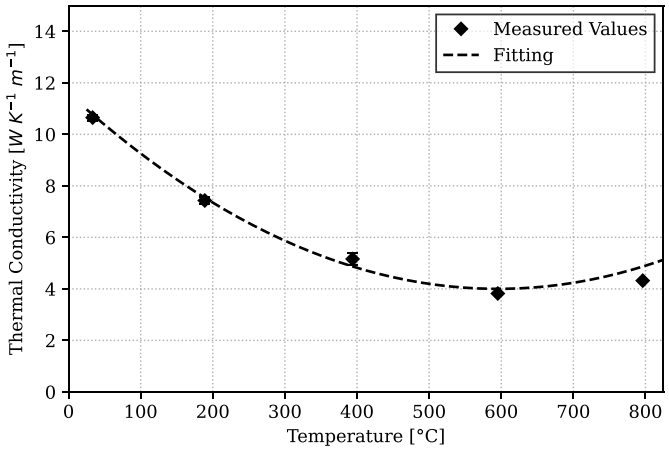

Fig. 1. Thermal conductivity for the 5CAC castable as a function of temperature [4].

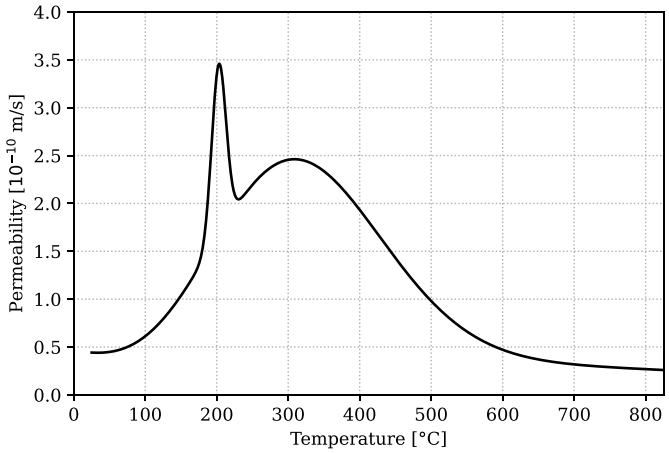

Fig. 2. Dynamic permeability values for the 5CAC composition [4].

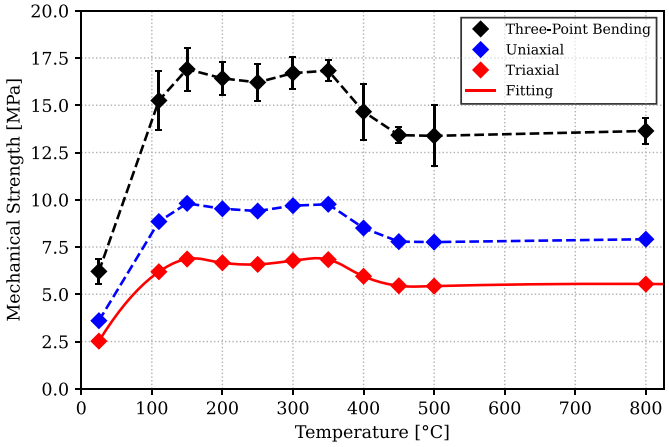

Fig. 3. Mechanical strength conversion showing the values of σ_{3p}, σ_{uni} and σ_{tri} [4].

application. To do this, a novel methodology for comparison among different curves is proposed, considering important aspects such as drying, probability of mechanical failure (resistance ratio) and consumed energy.

2. Materials and methods

2.1. Materials and properties

The selected material was a self-flowing high-alumina cement-bonded castable, which will be referred as 5CAC as it contains 5% mass content of calcium aluminate cement. The raw materials used, the mass fraction and the suppliers can be found in Ref. [4].

The composition was obtained considering the Andreassen particle packing model ($q = 0.21$) [6]. To prepare the material, a mixture of the dry powder was homogenized in a rheometer [7] and then it was shaped into 50 mm diameter and 50 mm height cylinders used for TGA [8,9]. 25 × 25 × 150 mm samples were used to evaluate the mechanical strength, 223 × 114 × 64 mm bricks for the thermal conductivity, and 38.2 mm diameter by 22 mm height cylinders for the permeability measurement. Afterwards, they were cured at 30 °C/24 h at 90% relative humidity, dried at 110 °C/24 h and then all the samples, except the ones used for TGA, were pre-fired in temperatures ranging from 300 to 800 °C/5 h.

Following the process described in detail in Ref. [4], the thermal conductivity and heat capacity were measured using the hot wire technique (ISO 8894-2) [10,11] and the permeability at room temperature was obtained following ASTM C577 [12,13] with samples dried at 110 °C. Moreover, the castable density was assessed according to ASTM C830-00 and the mechanical strength was obtained under three-point bending tests (ASTM C583-15) at a loading rate of 12.9 N/s.

Fig. 1 shows the values measured for the thermal conductivity, whereas Fig. 2 shows the measured values and an extrapolation of the permeability as a function of temperature based on the results of hot air flow rate attained by Ribeiro [14,15]. A comprehensible explanation of the adopted procedure can be found in Ref. [4].

Furthermore, the resistance ratio parameter, ξ, was used to compare the local mechanical strength of the refractory as a function of temperature (σ_{tri}) with the triaxially generated vapor pressure within the material ($P_{v_{max}}$), which can be defined as:

$$\xi = \frac{P_{v_{max}}}{\sigma_{tri}} \tag{1}$$

The values used for σ_{tri} were obtained based on a three-point bending test result, which was transformed into uniaxial mechanical resistance by using the Weibull modulus (m = 10.1, measured after curing for 24 h at 30 °C and drying for 24 h at 110 °C), and finally converted into the triaxial component via Hooke's law [4]. The Weibull modulus was measured after testing 30 samples at the green state, and assuming $\nu = 0.15$ based on former works for similar castables carried out by the research group.

Fig. 3 shows every result for the conversion methodology. The black markers indicate the measured values, alongside the standard deviation. The blue ones present those values transformed into the uniaxial component and the red points indicate the final values of the conversion. The red line shows the interpolated continuous function that was used to compute the resistance ratio as a function of the temperature range.

2.2. Numerical model

The numerical model used in this work was based on Bažant et al. [16,17] and Gong et al. [18–20], in which a single fluid phase represents both liquid water and steam. The resulting system of equations was solved by the finite element method, conversely to other studies developed recently that consider each fluid individually (dry air, water vapor, liquid water) [21,22].

Experimentally measured properties were inserted into the model aiming to evaluate a material as close as possible to a real one. Other properties needed by this system, which are not listed, were taken from an earlier work developed by the research group [23].

The numerical formulations are shown by Equations (2) (mass

Table 1
Properties and parameters used in the model.

Property	Unity	Value
Density, ρ	Kg m^{-3}	Measured
Hydraulic Permeability, a	m s^{-1}	Measured
Thermal Conductivity, k	W m^{-1} K^{-1}	Measured
Chemically Bound Water, w_d	Kg m^{-3}	Measured
Sorpted Water (Free Water), w	Kg m^{-3}	Adapted from [19]
Specific Heat of Water, C_w	J Kg^{-1} K^{-1}	4100
Adsorption Latent Heat, C_a	J Kg^{-1} K^{-1}	Adapted from [23,25]
Thermal Exchange Coefficient, B_t	W m^{-2} K^{-1}	Adapted from [19]
Mass Exchange Coefficient, B_w	s m^{-1}	$1 \cdot 10^{-6}$
Environment Temperature, T_{en}	°C	25
Environment Vapor Pressure, P_{ven}	Pa	2850
Emissivity, ε	–	Adapted from [24]

taken from published works by Gong et al. [19], Moreira [23] and Santos et al. [24].

An open source finite element model framework, FEniCS, was the numerical tool used to solve the system of equations. For the input of the equations in the software code, the system had to be transformed in the weak formulation [26–29], as follows,

$$\int_\Omega \frac{dw}{dt}\, v_1\, d\Omega + \int_\Omega \frac{d\dot{w}}{dt}\, v_1\, d\Omega - \int_{\Omega g} \frac{a}{g}\, \langle \nabla P, \nabla v_1 \rangle\, d\Omega - \int_\Gamma B_w\, (P_v - P_{ven})\, v_1\, d\Gamma = 0 \tag{4}$$

$$\int_\Omega \rho\, C_p\, \frac{dT}{dt}\, v_2\, d\Omega + \int_\Omega k\, \langle T, v_2 \rangle\, d\Omega - \int_\Omega C_a\, \frac{dw}{dt}\, v_2\, d\Omega + \int_\Omega C_w\, \frac{a}{g}\, \langle P_v, T \rangle\, v_2\, d\Omega - \int_\Gamma \sigma\, \varepsilon\, (T_{en}^4 - T^4)\, v_2 d\Gamma + B_t\, (T_{en} - T)\, v_2\, d\Gamma = 0 \tag{5}$$

balance) and 3 (energy balance).

$$\underbrace{\frac{dw}{dt}}_{a.1} = \underbrace{\nabla\cdot\left(\frac{a}{g}\nabla P_v\right)}_{a.2} + \underbrace{\frac{dw_d}{dt}}_{a.3} \tag{2}$$

$$\underbrace{\rho C_p \frac{dT}{dt}}_{b.1} = \underbrace{C_a \frac{dw}{dt}}_{b.2} - \underbrace{C_w \frac{a}{g}(\nabla P_v \cdot \nabla T)}_{b.3} + \underbrace{\nabla\cdot(k\nabla T)}_{b.4} \tag{3}$$

In Equation 2, (a.1) describes the variation in the free and adsorbed water with time, (a.2) the divergent of Darcinian flux and (a.3) the variation of chemically bound water with time. In Equation 3, (b.1) represents the variation of the thermal energy within the domain, (b.2) the energy consumed by water evaporation, (b.3) the thermal flux by convection and (b.4) the divergent of the Fourier flux. A more detailed description of the model used can be found in Ref. [5].

The boundary conditions on the heated surface describe the temperature as a function of time following a given drying profile. Convective and radiating effects on the thermal transfer at the cold surface, and the vapor transport on both sides were considered by Robin boundary conditions as described in Ref. [4].

All used properties are presented in Table 1. Some of them were

An open source finite element model framework, FEniCS, was the numerical tool used to solve the system of equations. For the input of the equations in the software code, the system had to be transformed in the weak formulation [26–29], as follows,

Furthermore, the simulation-specific parameters assumed a timestep of 15 s and a linear element on mono-dimensional mesh, while using a Newtonian solver for non-linear problems.

2.3. Simulation setup

Aiming to evaluate the use of a constant heating rate while drying the refractory castables, the following values were assumed for the heating schedules.

1. Initial temperature: 25 °C
2. Final temperature: 925 °C
3. Continuous heating rates: 50, 75 or 100 °C/h

The heating curve was built in such a way that it started at 25 °C, increasing linearly according to the selected heating rate up to the plateau temperature. It was then held for 30 h, and finally heated up with the same rate as before, up to the final temperature of 925 °C.

The geometry of interest was the lining of a steel ladle, thoroughly described in Ref. [4], which was based in the work by Santos et al. [24]. The ceramic lining had four different layers: (I) working, (II) permanent, (III) insulating and (IV) metallic shell. Each of them had different

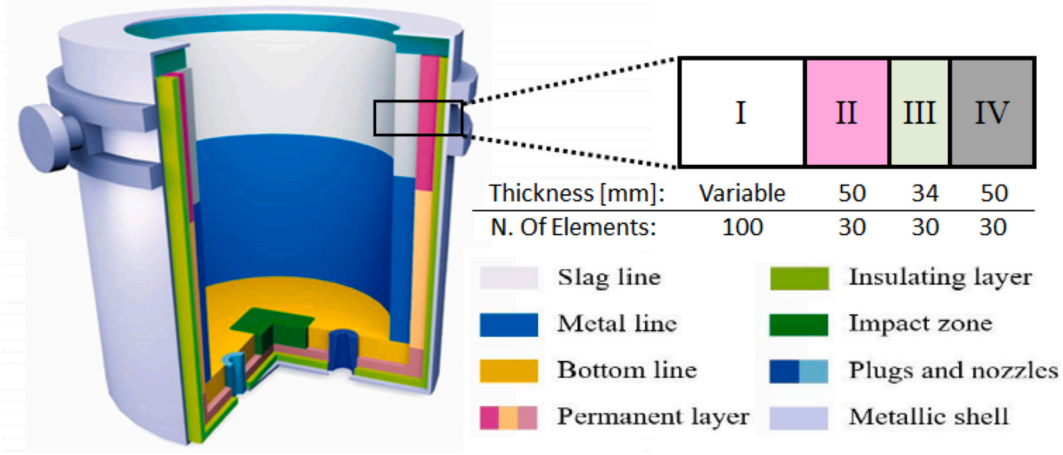

Fig. 4. Evaluated geometry, adapted from Ref. [24].

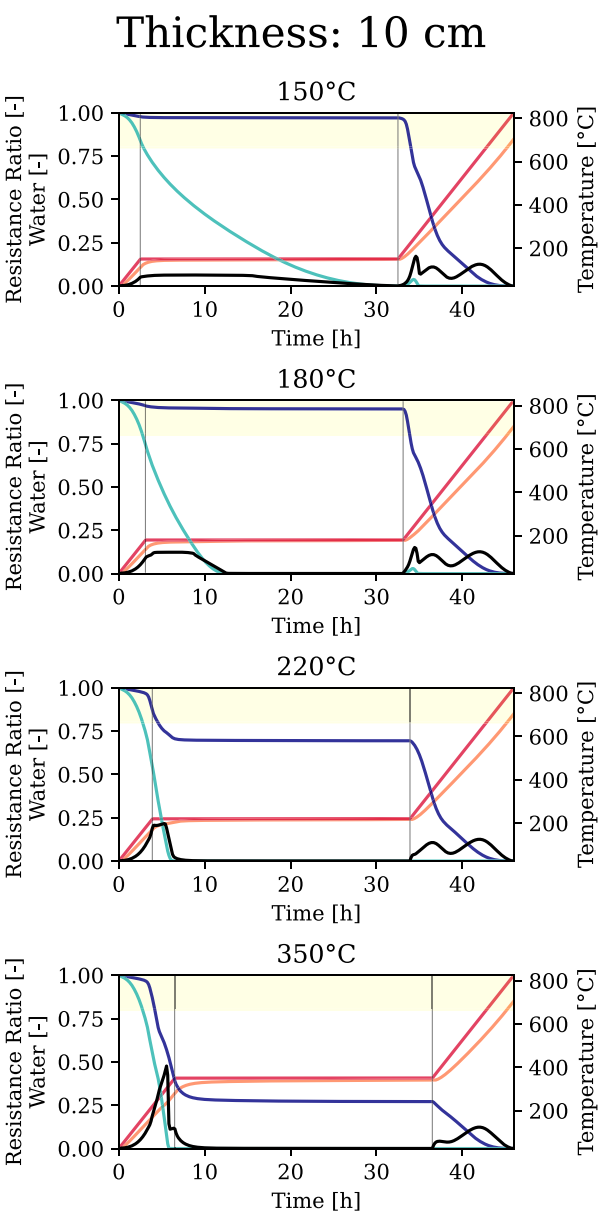

Fig. 5. Maximum resistance ratio (black), free adsorbed water (cyan), chemically bound water (blue), heat-up curve (red) and minimum temperature (orange) for the working layer of 10 cm thickness as a function of time. Each graph describes the behavior for different plateau temperatures, ranging from 150 °C to 350 °C at a heating rate of 50 °C/h for the ramps. (For interpretation of the references to colour in this figure legend, the reader is referred to the Web version of this article.)

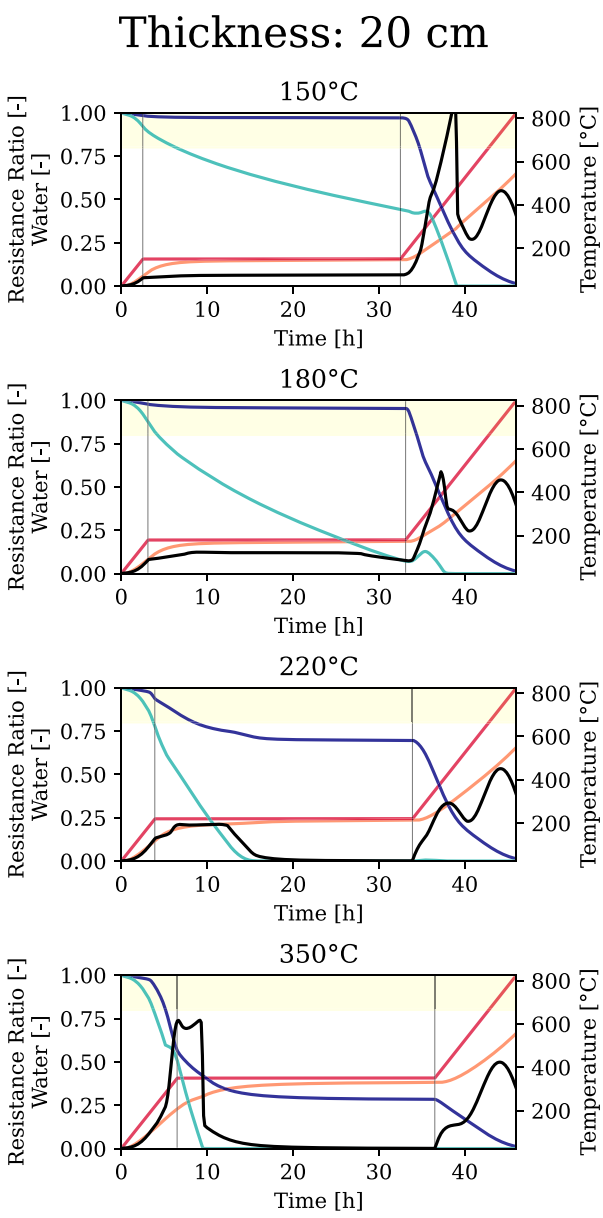

Fig. 6. Maximum resistance ratio (black), free adsorbed water (cyan), chemically bound water (blue), heat-up curve (red) and minimum temperature (orange) for the working layer of 20 cm thickness as a function of time. Each graph describes the behavior for different plateau temperatures, ranging from 150 °C to 350 °C at a heating rate of 50 °C/h for the ramps. (For interpretation of the references to colour in this figure legend, the reader is referred to the Web version of this article.)

thicknesses and were discretized in the model with a specific number of elements that can be found in Fig. 4.

The materials properties for each layer can be found in Ref. [4]. The working layer was a 5CAC castable. The following ones, permanent, insulating and metallic shell were comprised of high alumina, insulating alumina and carbon steel, respectively.

Based on the results of the former work [4], the authors decided to keep the values of both thermal conductivity and permeability as a function of temperature, as these are not only the most influential material properties in the drying model used, but also because results have shown the importance of carrying out the measurement of physical properties as close as possible to the reality. Additionally, they also take into consideration a likely representation of the dynamic effects of phase and microstructure changes during heating.

Regarding boundary conditions, the heating curve was applied to the hot face of layer I, whereas the heat was released at the cold side of layer IV. As only layer I goes through the drying process, the permeability boundary conditions for the transport of moisture between such a layer was considered at the hot face, and between layers I and II. The latter is associated to the mass transport of vapor between the layers due to a non-perfect coupling at the lining interface.

Moreover, at the initial stage of the simulations, the temperature and partial vapor pressure of water for every element was defined to be 25 °C and 2850 Pa, respectively. In addition, the initial free adsorbed water content was in equilibrium with these values for the entirety of the working layer.

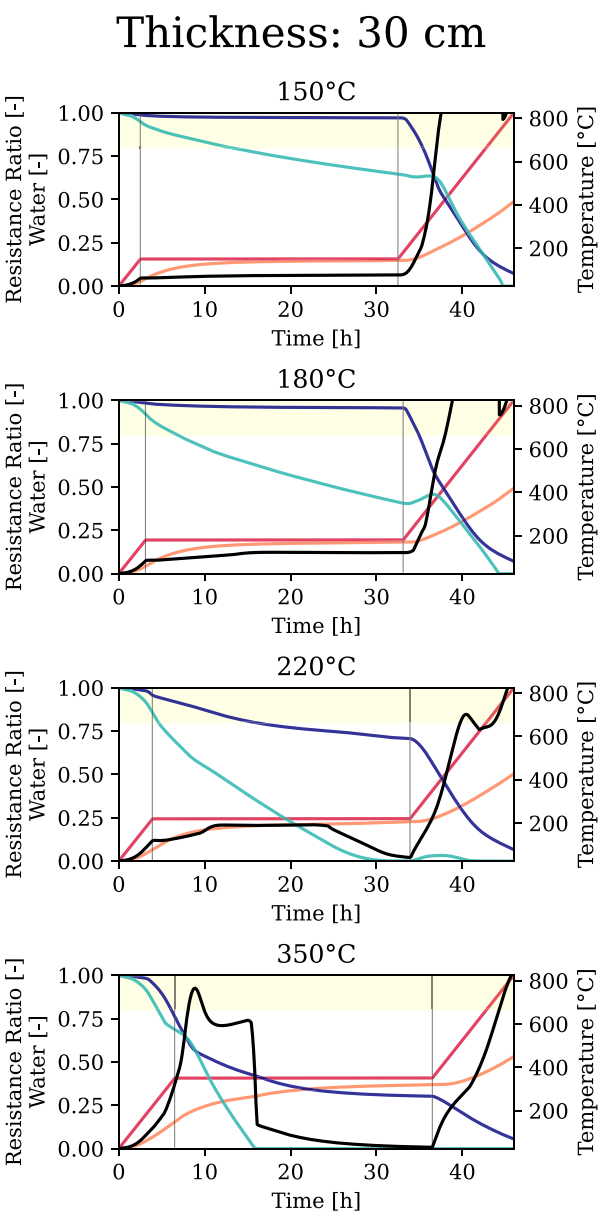

Fig. 7. Maximum resistance ratio (black), free adsorbed water (cyan), chemically bound water (blue), heat-up curve (red) and minimum temperature (orange) for the working layer of 30 cm thickness as a function of time. Each graph describes the behaviour for different plateau temperatures, ranging from 150 °C to 350 °C at a heating rate of 50 °C/h for the ramps. (For interpretation of the references to colour in this figure legend, the reader is referred to the Web version of this article.)

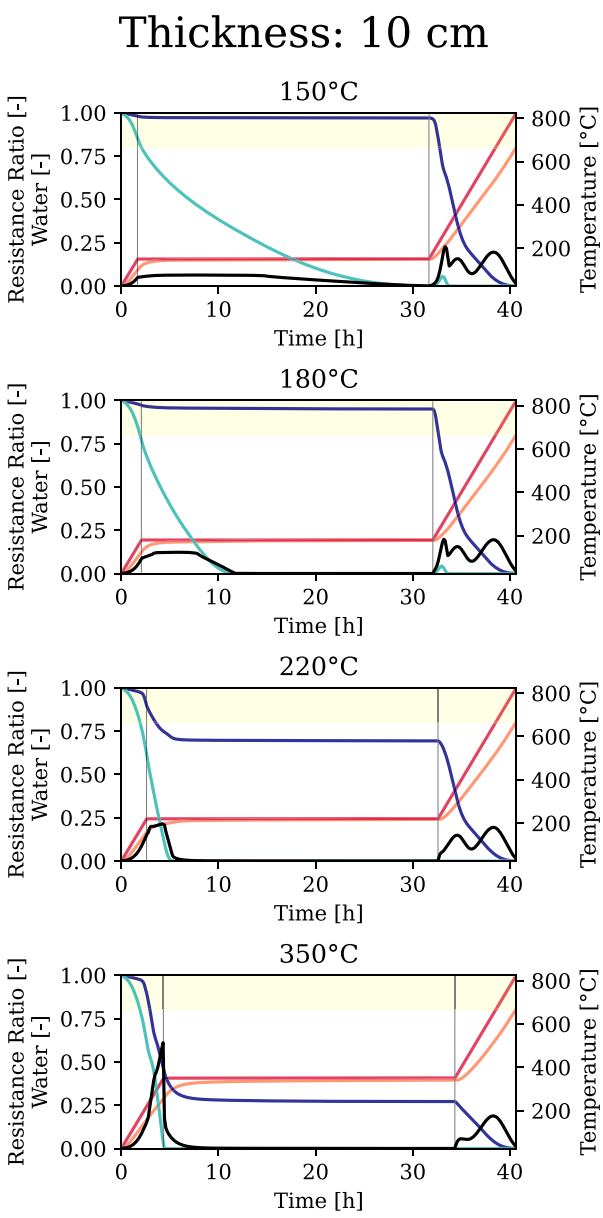

Fig. 8. Maximum resistance ratio (black), free adsorbed water (cyan), chemically bound water (blue), heat-up curve (red) and minimum temperature (orange) for the working layer of 10 cm thickness as a function of time. Each graph describes the behavior for different plateau temperatures, ranging from 150 °C to 350 °C at a heating rate of 75 °C/h for the ramps. (For interpretation of the references to colour in this figure legend, the reader is referred to the Web version of this article.)

2.4. Energy evaluation

As one of the goals of this study was to evaluate the energy consumption to compare the heating curves for all drying studies, a method to compute this value out of the simulation results, was developed.

The first approach was based on estimating the input flux in the hot face by integrating the heat flux (q) with respect to time and over the area of the surface, defining the input energy as E_{input},

$$E_{input} = \int_{t_0}^{t_f} \int_{\Gamma} -k\nabla T \, d\Gamma \, dt \tag{6}$$

The second methodology computed the consumed energy via the individual energy components of each layer, based on the equations already presented earlier (Equations (2) and (3)). For the working layer, both thermal and moisture components were computed similarly to the first approach taken, whereas for the following layers, only the thermal component was calculated, as those were considered water-free materials. The equations are described as

$$E_{st} = \int_{t_0}^{t_f} \int_{\Omega} \rho C_p \frac{dT}{dt} \, d\Omega \, dt \tag{7}$$

$$E_{dc} = \int_{t_0}^{t_f} \int_{\Omega} -C_a(T) \frac{dW}{dt} \, d\Omega \, dt \tag{8}$$

where, E_{st} is the total stored thermal energy within the monolithic lining, E_{dc} is the consumed energy for the evaporation and desorption processes

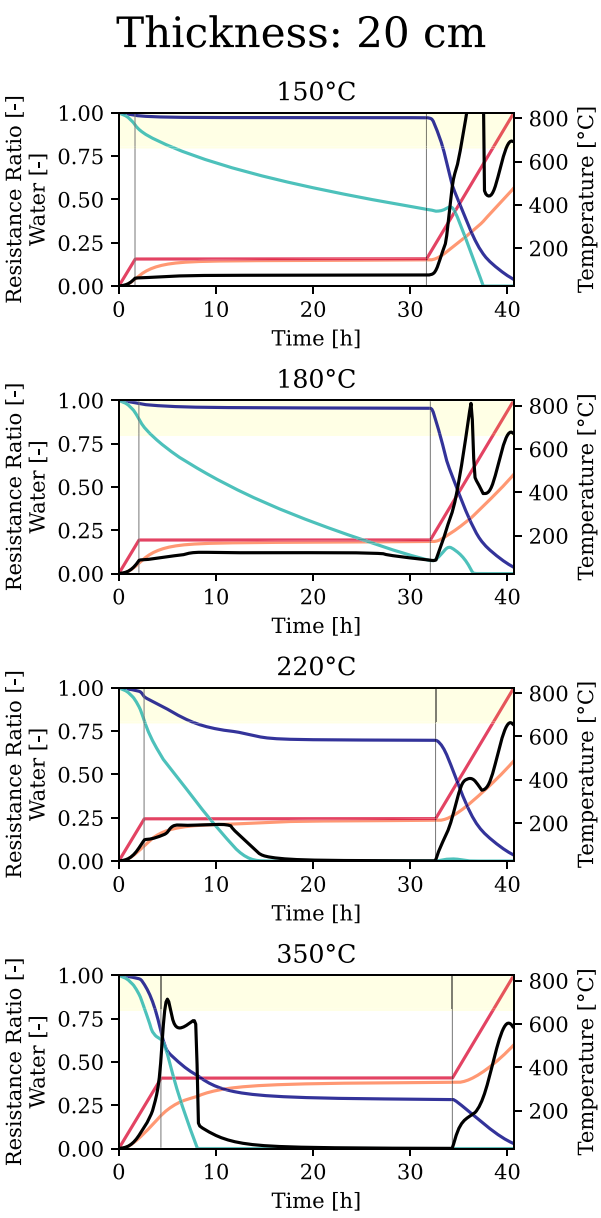

Fig. 9. Maximum resistance ratio (black), free adsorbed water (cyan), chemically bound water (blue), heat-up curve (red) and minimum temperature (orange) for the working layer of 20 cm thickness as a function of time. Each graph describes the behavior for different plateau temperatures, ranging from 150 °C to 350 °C at a heating rate of 75 °C/h for the ramps. (For interpretation of the references to colour in this figure legend, the reader is referred to the Web version of this article.)

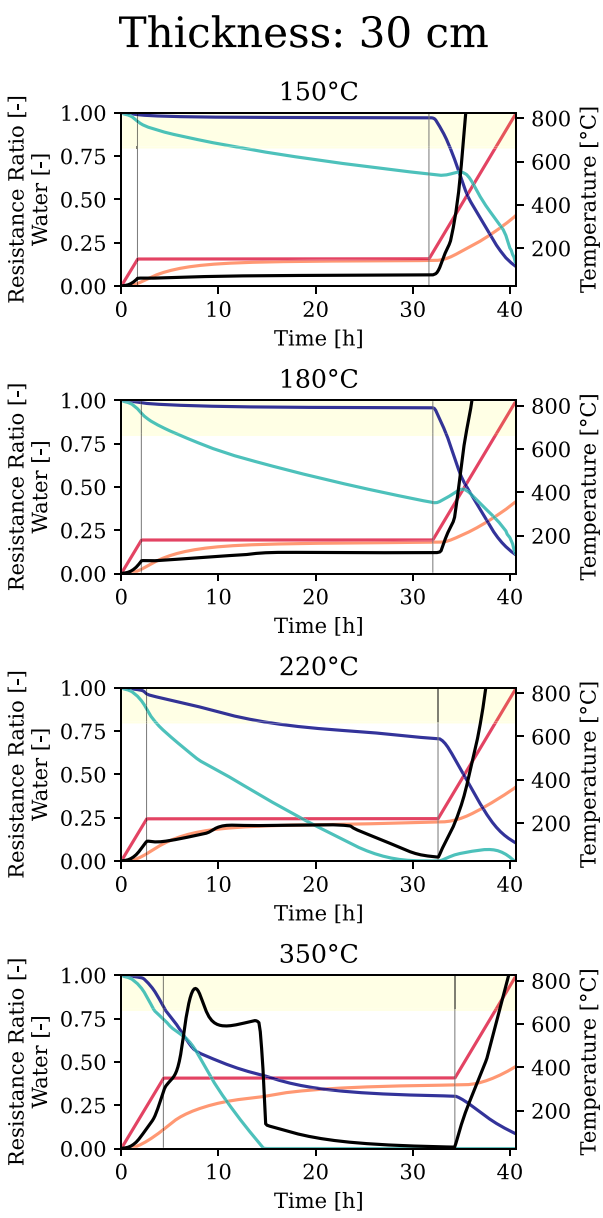

Fig. 10. Maximum resistance ratio (black), free adsorbed water (cyan), chemically bound water (blue), heat-up curve (red) and minimum temperature (orange) for the working layer of 30 cm thickness as a function of time. Each graph describes the behavior for different plateau temperatures, ranging from 150 °C to 350 °C at a heating rate of 75 °C/h for the ramps. (For interpretation of the references to colour in this figure legend, the reader is referred to the Web version of this article.)

of water. Finally, the energy that exited through the cold face, E_{cf}, was also calculated for the last element of the mesh and added to the total consumed energy in the process, as shown by

$$E_{cf} = \int_{t_0}^{t_f} \int_{\Gamma} B_t(T)(T_{en} - T) - \sigma\epsilon(T_{en}^4 - T^4)\, d\Gamma\, dt \tag{9}$$

$$E_{total} = E_{st} + E_{dc} + E_{cf} \tag{10}$$

For the third, and last, approach, the same values calculated for the former two methodologies were extracted as a heat flux value from within the simulation code by the specific FEniCS function (assemble()), which was then integrated in time in a similar way to the ones already described.

These three methodologies were compared to check whether they yielded the same value or not. The authors assessed the difference among them, which were lower than 3% of error, showing that they were all similar. Thus, the most straightfoward method of computing was chosen which was the extraction of these values by the FEniCS function (third approach), as it required the lowest number of operations.

3. Results

Figs. 5–7 show the different results for each of the simulations carried out for three different castable lining thicknesses at a heating rate of 50 °C/h. The profiles correspond to the resistance ratio, water content and temperature profiles as a function of time in the evaluated plateau temperatures.

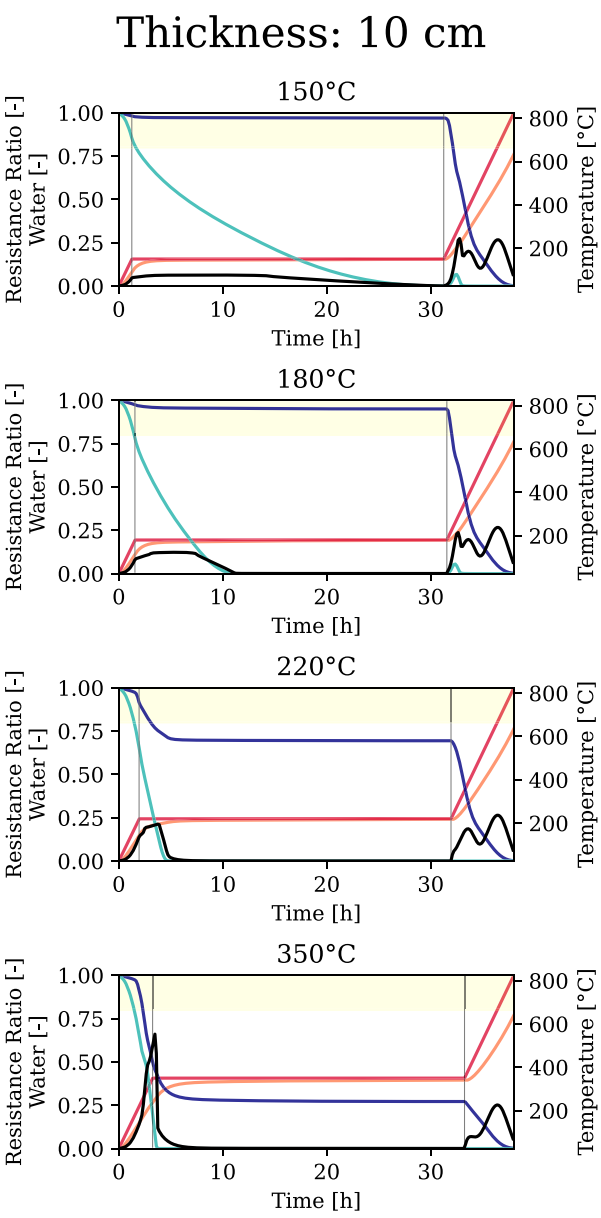

Fig. 11. Maximum resistance ratio (black), free adsorbed water (cyan), chemically bound water (blue), heat-up curve (red) and minimum temperature (orange) for the working layer of 10 cm thickness as a function of time. Each graph describes the behavior for different plateau temperatures, ranging from 150 °C to 350 °C at a heating rate of 100 °C/h for the ramps. (For interpretation of the references to colour in this figure legend, the reader is referred to the Web version of this article.)

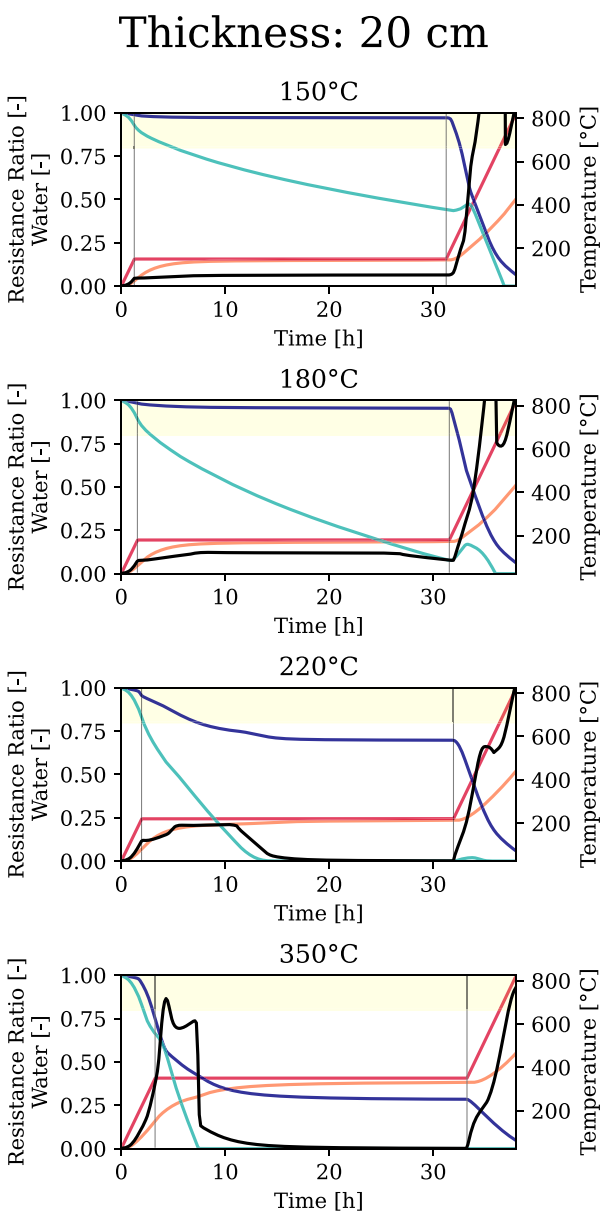

Fig. 12. Maximum resistance ratio (black), free adsorbed water (cyan), chemically bound water (blue), heat-up curve (red) and minimum temperature (orange) for the working layer of 20 cm thickness as a function of time. Each graph describes the behaviour for different plateau temperatures, ranging from 150 °C to 350 °C at a heating rate of 100 °C/h on the constant heating rate sections. (For interpretation of the references to colour in this figure legend, the reader is referred to the Web version of this article.)

It can be observed that, for the 10 cm thickness, there was no failure risk regardless of the plateau's temperature, as it can be noted by all values of the maximum resistance ratio below the threshold of 0.8. The plateau at 150 °C was too conservative in this specific scenario, as the total time for complete dry out the free water content increased when compared to the plateau at 180 °C, without major differences for the resistance ratio levels.

The likelihood of a shorter dwell time at 150 °C is highlighted when the working layer thickness increases to 20 cm, as this plateau temperature could not dry the free water completely. The same effect was also observed at 180 °C, although the final water content at the end of the plateau was not enough to increase the resistance ratio values above the limit. Although there was some residual pressure at the end of the process, it can be observed that the only source of water at this moment was a small quantity of a chemically bound one. This would not be enough to rise the pressure at risk levels, therefore it can be considered that the material was dried. For the 220 °C plateau, the behavior was very similar to the 10 cm thickness. Nevertheless, the extent of the obtained pressure plateau increased from nearly 4 h to about 15 h. For the plateau at 350 °C, the same behavior related to the occurrence of a pressure peak before the hot faces reached the holding temperature, was observed.

None of the simulations completed the heating schedule safely when the thickness increased to 30 cm, as the maximum resistance ratio calculated exceeded the safety factor. Although the free water could be completely removed for 30 h plateaus above 200 °C, there was a pressure build-up from the release of chemically bound water at high temperatures, making them impractical to provide safe drying. The reason of the high pressure values was due to Antoine's correlation which is

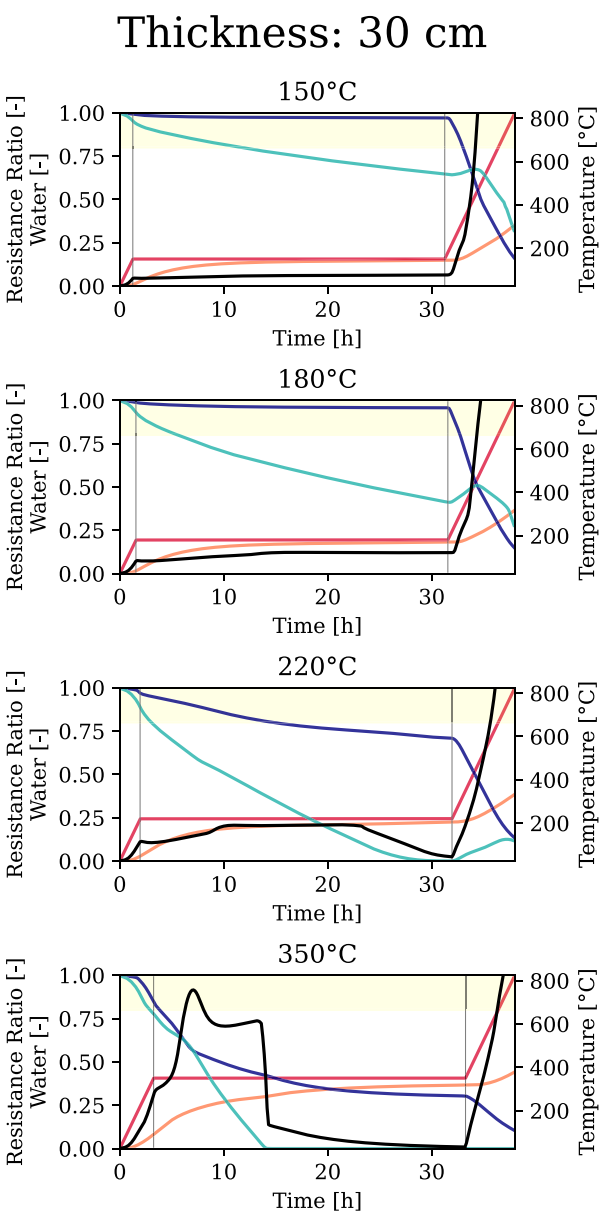

Fig. 13. Maximum resistance ratio (black), free adsorbed water (cyan), chemically bound water (blue), heat-up curve (red) and minimum temperature (orange) for the working layer of 30 cm thickness as a function of time. Each graph describes the behaviour for different plateau temperatures, ranging from 150 °C to 350 °C at a heating rate of 100 °C/h on the constant heating rate sections. (For interpretation of the references to colour in this figure legend, the reader is referred to the Web version of this article.)

described by Equation (11), where P_s is the pressure of saturation, A, B, C and D are experimental fitting parameters for specific substance, and T is the temperature. As can be calculated the saturation pressure increases exponentially with the temperature, increasing the risks of failure.

$$P_s = A * 10^{\left(B - \frac{C}{D+T}\right)} \tag{11}$$

For most of the results, the pressure levels at the plateaus were almost constant and similar to the ones for a heating rate of 50 °C/h, when the slope rates increased to 75 °C/h and 100 °C/h (Figs. 8–13).

The simultaneous release of the free and chemically bonded water is an important effect that can be clearly observed for the dwell time at 350 °C in Figs. 9, 10 and 13. The water vapor content increased,

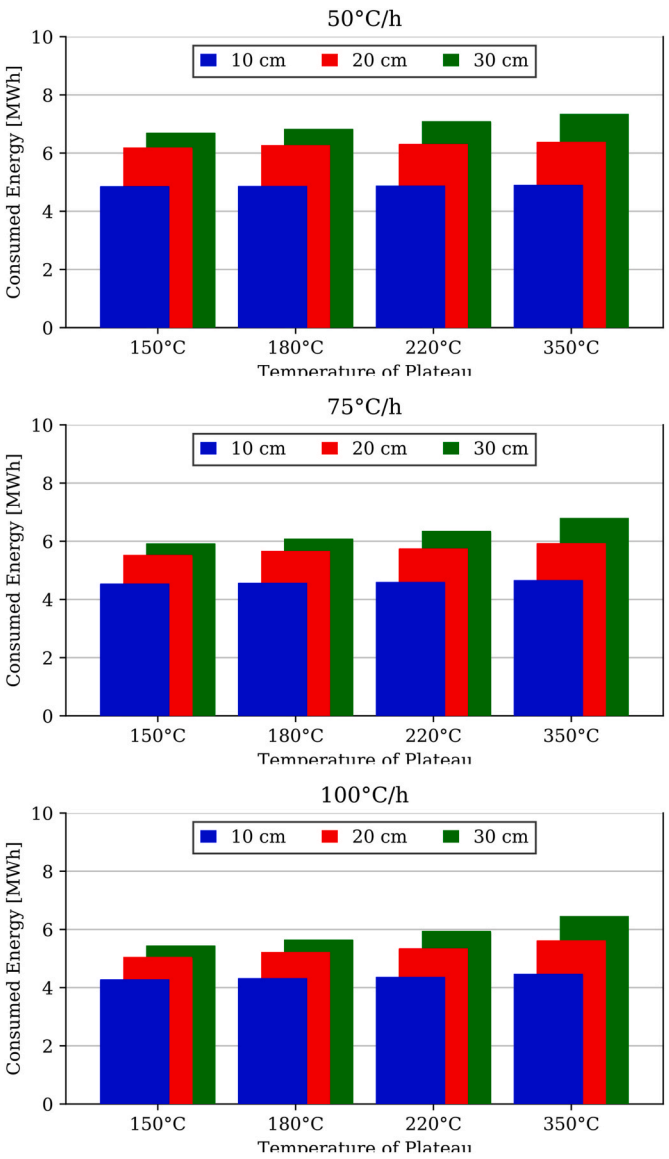

Fig. 14. Energy consumption for all simulated cases gathered by the heating rate.

resulting in a higher and faster pressure build-up than observed when they were released separately.

The independent withdrawal of these different moisture sources should be favored by designing new heat-up curves, mainly via two different temperature holding times. The selected temperatures should be lower than the ones of the decomposition of the binders' hydrates, which is close to 350 °C for this specific castable. In this case, a first plateau at 180 °C can allow the drying of free adsorbed water while keeping the chemically bound one content nearly constant. Moreover, none of the simulations considering a thickness of 30 cm dried safely, suggesting that the drying of a material with such a thickness might require a longer plateau or a more complex heating curve.

These highlights might not lead to different procedures than those carried out in practice, but as far as the authors are aware, the present methodology enables us to visualize and suggest likely novel dry-out curves assuring safety and shorter time.

In parallel to the analysis of pressure build-up behaviour in the process, this study compared the energy efficiency associated to each of these heating curve cases analyzed. The energy efficiency is linked to the industrial goals of reducing environmental impacts and selecting the best heating curve has a great effect on the total energy consumption

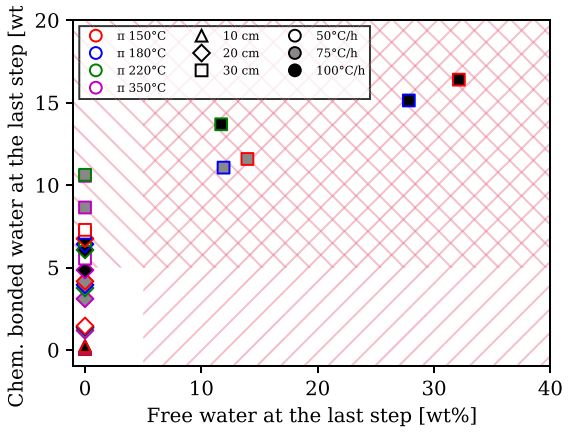

Fig. 15. Step 1 of the selection methodology. The x-axis describes the normalized amount of free water at the last time step, whereas the y-axis shows the amount of chemically bound water at the same moment. The red hashed background indicates the region in which the simulation results do not fulfill the selection condition (residual water <5% of the initial value). The letter π indicates the temperature of the plateau. (For interpretation of the references to colour in this figure legend, the reader is referred to the Web version of this article.)

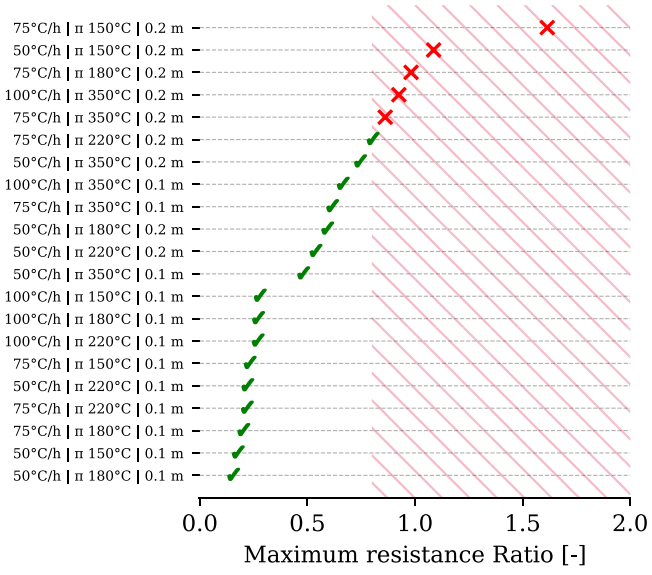

Fig. 16. Step 2 of the proposed methodology. The simulations are listed from the lowest to the highest resistance ratio, with a threshold at resistance ratio of 0.8 in order to define which simulations had safe drying.

and costs, especially on a steel ladle.

The results for the energy consumption calculated for every case previously analyzed can be found in Fig. 14.

It can be observed that the results followed a common trend, that can be described by: (i) the higher the heating rate, the lower the energy consumption as the heating time is shorter, (ii) the thicker the working layer, the more energy is used and, (iii) plateaus at high temperatures consumed more energy than those at lower ones as the material has to be kept in a hot environment for longer periods.

These results cannot lead to a comparative basis on which the scenario fits best the industry goals. That is why a "curve selection methodology" was defined, which comprised three different steps that are described next.

The first one evaluated the different curves checking whether or not

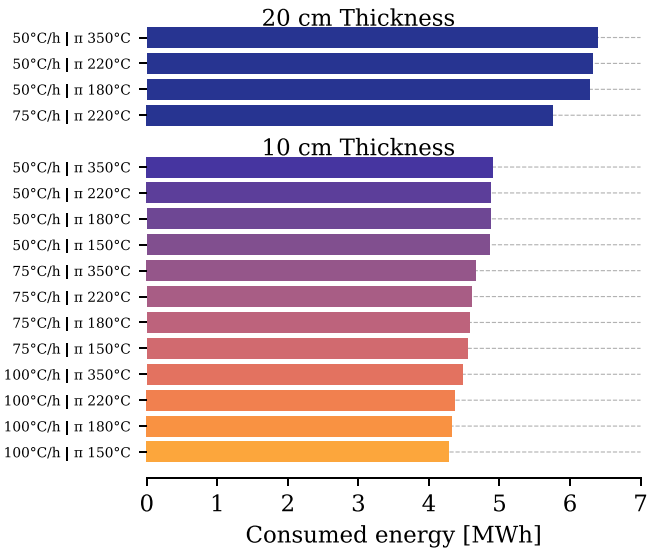

Fig. 17. Step 3 of the proposed methodology where the remaining heating profiles are ranked according to the energy consumption.

the castable was completely dry at the end of the process. Herein, the definition of a dried material is reaching less than 5% of residual free and chemically bound water related to the total initial amount. These cases are shown in Fig. 15 by the markers that are outside the hatched area, which is the region where remaining water is above this threshold for each different source. The graph shows that none of the 30 cm thickness simulations passed the first selection step, and therefore, these cases would require a more complex heating method or a longer holding time to safely dry them, which is compatible with what was also observed in Figs. 7, 10 and 13.

The second step tackled only the remaining profiles (outside the dashed area) and it evaluated whether their maximum resistance ratio crossed over the safety threshold of 0.8 (Fig. 16). After this step, only the 30 cm thickness simulations were rejected, indicating that all the conditions where the castable thickness was 10 cm were safely dried. Then, there was one specific simulation in which the maximum resistance ratio was slightly under the threshold (heating rate of 75 °C/h, plateau temperature of 220 °C and thickness of 20 cm). Analyzing only the absolute value, it was below 0.8 but it should be carefully evaluated whether the end-users could decide or not to take that risk.

Finally, the third step ranked the last group of cases according to the total energy consumption (Fig. 17). For the 10 cm thickness, the best options were using 100 °C/h heating rate and plateaus at 150 °C or 180 °C. Whereas for 20 cm thickness, the optimal ones were 75 °C/h with the plateau at 220 °C or 50 °C/h with a plateau at 180 °C. As it was already discussed, the plateaus at 180 °C showed similar features as those at a lower temperature. Therefore, the latter would be selected for a thickness layer of 10 cm. Furthermore, the heating profile of the lowest energy consumption for the 20 cm cases was the one closer to the maximum resistance ratio threshold in Fig. 16, and the end-user could choose this case as its second best curve.

The suggested methodology shows different steps in which the evaluated curves can be filtered out according to the fundamental concepts that matter in their final application. Although the selection presented in this work excludes the evaluation of total heating time as a parameter, as most of them have the same total duration, this factor could also be considered by the end-user, thus proposing a more complex ranking system. In addition, the weights for each index could be defined differently depending on the requirements for a given application.

4. Conclusions

This work answered the question "what are holding times for?" by proposing the analysis of different heating curves for drying a specific refractory material. The results showed that the temperature and the duration of the plateaus were of the greatest importance as they (i) can allow the release of free water and (ii) stabilize the pressure to a constant maximum value. The holding times at 150 °C were not as promising for this specific castable as only a 30 °C increase in this temperature allowed a much faster drying. A single plateau at 350 °C is not useful for lower thicknesses (10 cm) as the resistance ratio peak was already reached at the beginning of the dwell time.

Increasing the castable wall thickness to values up to 30 cm requires longer holding times or even more complex curves than the ones presented, as it was not possible to completely withdraw the moisture without risk of explosion. Yet, it was clear that for optimal heating, the separation of the withdrawal of water from free adsorbed (at a plateau near 180 °C) and chemically bound sources (temperature plateau in the 300–350 °C) can be beneficial for a safer and faster drying. These more complex heating profiles will be investigated in future works of the research group.

Finally, computing the total consumed energy during the entire process can allow the end-user to develop a more robust ranking system to choose the most suitable heating profile. In this case, the authors decided, in order, to check whether the material did not fail, if it was dried by the end of the process (5 wt% of both free and chemically bonded water) and consumed the least amount of energy.

Declaration of competing interests

The authors declare that they have no known competing financial interests or personal relationships that could have appeared to influence the work reported in this paper.

Acknowledgments

This study was financed in part by the Coordenação de Aperfeiçoamento de Pessoal de Nível Superior - Brasil (CAPES) - Finance Code 001. The authors would like to thank the Conselho Nacional de Desenvolvimento Cientifico e Tecnologica – CNPq (grant number: 134347/2019-6) and Fundação de Amparo à Pesquisa do Estado de São Paulo - FAPESP (grant number: 2021/00251-0) for supporting this work. Finally, the authors are thankful for the support of FIRE.

References

[1] C. Schacht, Refractories Handbook, oCLC: 910581448, CRC Press, Hoboken, 2004, ISBN 978-0-203-02632-8.
[2] W. Lee, W. Vieira, S. Zhang, K. Ahari, H. Sarpoolaky, C. Parr, Castable refractory concretes, Int. Mater. Rev. 46 (3) (2001) 145–167.
[3] A.P. Luz, M.A.L. Braulio, V.C. Pandolfelli, Refractory Castable Engineering, Goller Verlag GmbH, Baden-Baden, 2015, ISBN 978-3-87264-004-8.
[4] T.M. Cunha, M.H. Moreira, M.F. Santos, A.P. Luz, V.C. Pandolfelli, Drying behavior of steel-ladle lining refractory castables under continuous heating rate, Ceram. Int. 48 (1) (2022) 1142–1151.
[5] M.H. Moreira, S.D. Pont, R.F. Ausas, A.P. Luz, T.M. Cunha, C. Parr, V.C. Pandolfelli, Main trends on the simulation of the drying of refractory castables - Review, Ceram. Int. 47 (20) (2021) 28086–28105.
[6] A.P. Luz, M.H. Moreira, C. Wöhrmeyer, C. Parr, V.C. Pandolfelli, Drying behavior optimization of dense refractory castables by adding a permeability enhancing active compound, Part A, Ceram. Int. 45 (7) (2019) 9048–9060.
[7] R. Pileggi, V.C. Pandolfelli, A.E. Paiva, J. Gallo, Novel rheometer for refractory castables, Am. Ceram. Soc. Bull. 79 (1) (2000) 54–58.
[8] M.D.M. Innocentini, F.A. Cardoso, M.M. Akyioshi, V.C. Pandolfelli, Drying stages during the heating of high-alumina, ultra-low-cement refractory castables, J. Am. Ceram. Soc. 86 (7) (2003) 1146–1148.
[9] A. Santos, A. Paiva, A.P. Luz, V.C. Pandolfelli, Influence of $MgCl_2$ and $CaCl_2$ salts on MgO hydration behaviour, Ceramica 64 (2018) 20–29.
[10] M. Akiyoshi, A. Christoforo, A.P. Luz, V.C. Pandolfelli, Thermal conductivity modeling based on physical and chemical properties of refractories, Ceram. Int. 43 (2016) 4731–4745.
[11] F. Arroyo, A. Christoforo, V. Salvini, P.I. Pelissari, V.C. Pandolfelli, A. Luz, C. Cardoso, Development of plaster foam for thermal and acoustic applications, Construct. Build. Mater. 262 (2020), 120800.
[12] M. Innocentini, M. Silva, B. Menegazzo, V.C. Pandolfelli, Permeability of refractory castables at high temperatures, J. Am. Ceram. Soc. 84 (2004) 645–647.
[13] M. Innocentini, R. Salomão, C. Ribeiro, F. Cardoso, V. Pandolfelli, R. Rettore, L. Bittencourt, Permeability of fiber-containing refractory castables - part 1, Am. Ceram. Soc. Bull. 81 (2002) 34–38.
[14] C. Ribeiro, M. Innocentini, V.C. Pandolfelli, Dynamic permeability behavior during drying of refractory castables based on calcium-free alumina binders, J. Am. Ceram. Soc. 84 (2004) 248–250.
[15] C.R. Oliveira, Effects of Temperature and Drying Additives in the Permeability of Refractory Castables, Dissertation (Master in Materials Science and Engineering), PPG-CEM UFSCar, São Carlos, Brazil, 2002 (In Portuguese).
[16] Z.P. Bažant, W. Thonguthai, Pore pressure in heated concrete walls: theoretical prediction, Mag. Concr. Res. 31 (107) (1979) 67–76.
[17] Z.P. Bažant, M. Jirásek, Creep and Hygrothermal Effects in Concrete Structures, 225, Springer Netherlands, Dordrecht, 2018, 978-94-024-1136-2 978-94-024-1138-6.
[18] Z.-X. Gong, A.S. Mujumdar, A model for kiln-drying of refractory concrete slabs, Dry. Technol. 11 (7) (1993) 1617–1639.
[19] Z.-X. Gong, A.S. Mujumdar, The influence of an impermeable surface on pore steam pressure during drying of refractory concrete slabs, Int. J. Heat Mass Tran. 38 (7) (1995) 1297–1303.
[20] Z.-X. Gong, A.S. Mujumdar, Development of drying schedules for one-side-heating drying of refractory concrete slabs based on a finite element model, J. Am. Ceram. Soc. 79 (6) (1996) 1649–1658.
[21] D. Gawin, F. Pesavento, B.A. Schrefler, What physical phenomena can be neglected when modelling concrete at high temperature? A comparative study. Part 1: physical phenomena and mathematical model, Int. J. Solid Struct. 48 (13) (2011) 1927–1944.
[22] D. Gawin, F. Pesavento, B.A. Schrefler, What physical phenomena can be neglected when modelling concrete at high temperature? A comparative study. Part 2: comparison between models, Int. J. Solid Struct. 48 (13) (2011) 1945–1961.
[23] M.H. Moreira, A.P. Luz, T.M. Cunha, H. Lemaistre, J. Auvray, C. Parr, R.F. Ausas, V.C. Pandolfelli, Practical numerical simulation and experimental setup for speeding up the drying behavior of calcium aluminate cement (CAC)-bonded refractory castables, in: UNITECR'19. Proc. Unified Int. Tech. Conf. On Refractories. 16 Th Biennial Worldwide Congress. "Refractories for the Future", 1, 2019, pp. 167–169.
[24] M. Santos, M. Moreira, M. Campos, P.I. Pelissari, R. Angélico, E. Sako, S. Sinnema, V.C. Pandolfelli, Enhanced numerical tool to evaluate steel ladle thermal losses, Ceram. Int. 44 (2018) 12831–12840.
[25] M.H. Moreira, Use of a Numerical Model to Optimize the Drying Heat-Up Curves of High-Alumina Castables, Monography (Bachelor in Materials Engineering), 2019. UFSCar (Federal University of São Carlos), São Carlos, Brazil. (In Portuguese).
[26] E. M. Cummings, Modeling the Cryosphere with FEniCS, arXiv:1609.02190 [physics] ArXiv: 1609.02190.
[27] A. Logg, G.N. Wells, DOLFIN: Automated finite element computing, ACM Trans. Math Software 37 (2) (2010) 1–28.
[28] H.P. Langtangen, A. Logg, Solving PDEs in python: the FEniCS Tutorial I, Springer Nature, 2017.
[29] M. Alnæs, J. Blechta, J. Hake, A. Johansson, B. Kehlet, A. Logg, C. Richardson, J. Ring, M. E. Rognes, G. N. Wells, The FEniCS project Version 1.5, Arch. Num. Softw. Vol 3.